Advanced Pharmaceutical Bulletin

Accepted Manuscript (unedited)

The manuscript will undergo copyediting, typesetting, and review of the resulting proof before it is published in its final form.

Research Article

How to cite this article:
Goodarzi Fard G, Abdolmaleki A, Asadi A, Zolfagharpour F, Nourizadeh E, Nahumi A, A. Ghanimi H. Investigating the Radioprotective Properties of C60 Fullerene Nanoparticles: Effects on Adipose-Derived Stem Cell Viability and Inflammatory Markers. Advanced Pharmaceutical Bulletin, doi: 10.34172/apb.46954

Investigating the Radioprotective Properties of C60 Fullerene Nanoparticles: Effects on Adipose-Derived Stem Cell Viability and Inflammatory Markers

Golnoosh Goodarzi Fard[1], Arash Abdolmaleki[*,1], Asadollah Asadi[2], Farhad Zolfagharpour[3], Ezzat Nourizadeh[2], Aida Nahumi[2], Hussein A. Ghanimi[4]

[1] Department of Biophysics, Faculty of Advanced Technologies, University of Mohaghegh Ardabili, Namin, Iran
[2] Department of Biology, Faculty of Science, University of Mohaghegh Ardabili, Ardabil, Iran
[3] Department of Physics, Faculty of Science, University of Mohaghegh Ardabili, Ardabil, Iran
[4] College of Nursing, University of Al-Ameed, Karbala, Iraq

ARTICLE INFO

Keywords:
Cytokines,
X-Rays,
Stem Cells,
Radiation Protection,
Nanostructures

Article History:
Submitted: December 21, 2025
Revised: May 10, 2026
Accepted: June 22, 2026
ePublished: June 29, 2026

ABSTRACT

Purpose: Radiation exposure triggers oxidative stress and inflammatory responses that contribute to cellular damage and hinder tissue regeneration. Developing effective radioprotective strategies is therefore essential for improving therapeutic outcomes in regenerative medicine. This study investigated the radioprotective effects of C60 fullerene nanoparticles on adipose-derived stem cells (ASCs) exposed to X-ray irradiation in vitro.
Methods: C60 nanoparticles were synthesized using the electric arc discharge method and characterized by FE-SEM, FTIR, and XRD, confirming their nanoscale size, spherical morphology, and high purity. ASCs were treated with varying concentrations of C60 (0, 5, 10, 15 µg/mL) before irradiation, and cell viability, oxidative stress, and inflammatory markers were evaluated.
Results: C60 treatment significantly improved cell viability compared with irradiated and untreated controls. Nitric oxide (NO), a major indicator of oxidative stress, decreased in a dose-dependent manner following nanoparticle administration. Additionally, the expression levels of pro-inflammatory cytokines IL-6 and TNF-α were markedly reduced, demonstrating the anti-inflammatory potential of C60 and its ability to mitigate radiation-induced cellular injury.
Conclusion: Overall, the findings indicate that C60 fullerene nanoparticles possess notable radioprotective properties, driven by their antioxidant and anti-inflammatory effects. Further research is required to elucidate their mechanisms of action and assess their potential applications in regenerative medicine and related biomedical fields.

***Corresponding Author**
Arash Abdolmaleki, E-mail: abdolmalekiarash1364@gmail.com, ORCID: 0000-0002-7454-8728

1. Introduction

Stem cells, defined by their capacity for self-renewal and differentiation into specialized cell types,[1] hold significant promise for tissue regeneration and medical therapy.[2,3] Among various sources, Mesenchymal Stem Cells (MSCs) have emerged as prime candidates for clinical applications [3]. While bone marrow has been a traditional source of MSCs, the invasive nature of marrow harvesting presents challenges.[4,5] Consequently, alternative sources like adipose tissue have gained prominence due to their accessibility and ease of isolation.[3] Adipose-derived Stem Cells (ASCs), particularly those from white adipose tissue (WAT), are abundant and possess significant plasticity, making them highly suitable for regenerative medicine and tissue engineering.[6-8] WAT is now understood not merely as an energy depot but as an active endocrine organ containing a rich cellular milieu, including adult mesenchymal stem cells.[7,8] The straightforward, non-invasive isolation of ASCs further supports their utility.

The therapeutic potential of ASCs in regenerative medicine is substantial, but their application, particularly in contexts involving radiation exposure, requires careful consideration.[9] Radiation therapy, while crucial for treating various conditions, can cause significant damage to healthy tissues, including stem cell populations, thereby compromising regenerative capacity. ASCs, despite their inherent resilience and regenerative capabilities, are not immune to the cytotoxic effects of ionizing radiation. DNA damage, loss of proliferative potential, and induction of apoptosis are well-documented consequences of radiation exposure in stem cells.[10,11]

Carbon nanomaterials typically exhibit dimensions between 1 and 100 nanometers, which leads to significant alterations relative to bulk materials. These changes include an increased surface-to-volume ratio, diverse nanostructural configurations, distinct optical characteristics, and varied chemical reactivity.[12]

Fullerenes are the 3rd allotropic shape of carbon, following graphite and diamond, and have been named after architect Buckminster Fuller, who created geodesic domes in the 1960s. Fullerenes are structurally defined by a fixed set of twelve pentagonal rings and an array of hexagonal rings whose quantity depends on the fullerene type, collectively forming a closed, spheroidal nanocage architecture exhibiting icosahedral symmetry.[13] Euler's theorem states that the surface of a sphere has to have precisely twelve pentagons.[14] According to the number of hexagons, molecules of various sizes are produced.[13] One of the characteristics of fullerenes is their hydrophobicity, and their solubility decreases as their size increases.[15] Fullerenes have an aromatic structure and are soluble in organic hydrocarbons and halogenated solvents.[16] In the structure of fullerenes, every carbon atom forms three covalent bonds with neighboring carbon atoms, exhibiting an sp^2 hybridization state.[13] C_{60} fullerenes are new allotropic forms of carbon with a spherical structure and a diameter of approximately 1 nanometer, which have their own unique physicochemical properties.[17] The C_{60} molecule does not exhibit superaromaticity, as it minimizes the presence of double bonds within its pentagonal rings, which hinders efficient electron delocalization. Consequently, it behaves as an alkene with electron deficiency, engaging in reactions with electron-donating species.[13] Fullerenes are potent antioxidants that respond easily and quickly with radicals that are free, which are frequently the root cause of cell harm or death. They operate as a "radical sponge" by neutralizing over twenty free radicals. And they have demonstrated to be one hundred times more efficient than existing main antioxidants like vitamin E.[13]

The present research intends to evaluate the potential radioprotective impact of fullerene nanoparticles (C60) on adipose-derived stem cells exposed to X-ray radiation in vitro. This study particularly investigates how exposure to fullerene nanoparticles influences cell viability, indicators of oxidative stress, and levels of key pro-

inflammatory mediators such as nitric oxide (NO), interleukin-6 (IL-6), and tumor necrosis factor-alpha (TNF-α). By analyzing these parameters, the study seeks to elucidate the mechanisms by which fullerene nanoparticles mitigate radiation-induced cellular damage and inflammatory responses, ultimately contributing to advancements in nanomaterial-based radioprotection strategies.

2. Materials and Methods

2.1. Synthesis of C_{60} Fullerene NPs

C_{60} was produced in this research utilizing an electric arc discharge process with graphite as its source. To prepare a colloidal solution of C_{60} fullerene nanoparticles, 50 mg of the synthesized particles were dispersed in 10 ml of olive oil. The mixture underwent ultrasonic treatment for 72 hours, followed by continuous stirring with a magnetic stirrer for an additional 48 hours. The resulting suspension was then centrifuged at 7000 rpm for 1 hour, and the collected supernatant was subsequently filtered through a 0.2 μm membrane to ensure purity.

2.1.1. Characterization of C_{60} Fullerene NPs

Comprehensive physicochemical characterization of the synthesized nanoparticles was performed utilizing advanced techniques including field emission scanning electron microscopy (FE-SEM) for detailed morphological assessment, Fourier-transform infrared spectroscopy (FTIR) for molecular functional group elucidation, and X-ray diffraction (XRD) to determine crystallographic structures.

2.2. Field Emission Scanning Electron Microscope

The morphological features, including size and geometry, of the synthesized C60 fullerene nanoparticles were examined by field emission scanning electron microscopy (MIRA3 TESCAN system). To examine the nanoparticles using FE-SEM, a specific amount of the nanoparticle dispersion in distilled water was applied onto a substrate coated with gold. Prior to imaging, the dried nanoparticles were sputter-coated with a fine gold layer to ensure proper electron conductivity during analysis. We applied the gold covering using BAL-TEC model SCD005 coating equipment from Zurich, Switzerland.

2.3. FTIR spectroscopy

FTIR analysis was employed to identify the chemical structure of the synthesized C_{60} fullerene nanoparticles using a Bruker Tensor 27 system (Biotage, Düsseldorf, Germany). For sample preparation, 2 mg of the nanoparticles were finely milled and mixed with 200 mg of potassium bromide (KBr), then the mixture was pressed into a transparent pellet suitable for spectroscopic evaluation. The spectrum of the prepared pellets was recorded utilizing 16 scans within the wavenumber interval from 400 to 4000 cm^{-1}.

2.4. X-ray diffraction

X-ray diffraction (XRD) analysis was employed to investigate the crystalline structure of the synthesized C60 fullerene nanoparticles. The crystalline structure of the nanoparticles was characterized by powder X-ray diffraction (XRD) utilizing a Bruker AXS D8 Advance diffractometer (Ettlingen, Germany). The XRD patterns of C60 fullerene nanoparticles were collected over the angular span of 20° to 80° using a diffractometer with Cu Kα radiation (k = 1.542 Å).

2.5. Cell viability assay

Cell cultures were established in 96-well microplates using a growth medium supplemented with 10% fetal bovine serum (FBS), and subsequently incubated at 37°C for 24 hours under standard conditions. After incubation, cells received treatment with fullerene at different doses (0, 5, 10, and 15 μg/ml) for 1 hour. Subsequently, the plate

was then placed under X-rays for 30 minutes before being assessed for cell survival using the MTT test. In summary, 20 µL of MTT solution at a concentration of 0.5 mg/mL (Sigma, MO, USA) was added to each well and incubated for a duration of three hours. To solubilize the formazan crystals, 200 µL of DMSO was introduced into each well, followed by a 5-minute incubation. The optical absorbance at 570 nm was precisely quantified using a microplate spectrophotometer calibrated for ELISA assays, ensuring accurate biophysical characterization of the sample. All experiments were performed three times independently (n = 3 independent biological replicates), with each condition tested in quadruplicate (4 technical replicates) within each independent experiment. Data are presented as mean ± standard deviation (SD) derived from the three independent experiments.

2.6. Nitric oxide assay

We used this method to measure the levels of nitric oxide (NO) in cell samples. Cells were seeded into 96-well plates containing culture medium supplemented with 10% fetal bovine serum and maintained at 37°C for a duration of 24 hours. Following incubation, cells were administered with varying concentrations of fullerene (0, 5, 10, and 15 µg/mL) for one hour, subsequently subjected to X-ray irradiation for a duration of 30 minutes. The supernatant was collected under a laminar flow hood and transferred to microtubes for analysis using a nitric oxide measurement kit (Navand-Salamat Lab Kit, Iran). To measure nitric oxide levels, cells (2×10^6) were washed with PBS (pH = 7.4), homogenized at a 1:1 ratio, and centrifuged at 14,000 rpm in a refrigerated centrifuge. The supernatant was harvested, and protein precipitation was initiated by mixing a 150 µL portion of the sample blended with 80 µL of Buffer A, followed by the addition of 80 µL of Buffer B, in accordance with the manufacturer's protocol. After thorough vortexing, the mixture was centrifuged under the same conditions for 10 minutes, and the resulting supernatant was used as the sample. To determine nitric oxide concentration, the samples were combined with reagents R1 and R2, as per the kit protocol, and transferred to a 96-well microplate. After incubation at ambient temperature in the absence of light, absorbance readings were obtained at a wavelength of 570 nm. A calibration curve was generated using a nitrite reference solution, from which the nitric oxide concentration was subsequently derived. All experiments were performed three times independently (n = 3 independent biological replicates), with each condition tested in quadruplicate (4 technical replicates) within each independent experiment. Data are presented as mean ± standard deviation (SD) derived from the three independent experiments.

2.7. IL-6 assay

IL-6 concentrations in cellular samples were quantified utilizing an IL-6 assay kit (Karmania Pars Gene, Iran). Cells were seeded into 96-well culture plates containing medium supplemented with 10% fetal bovine serum and maintained under standard physiological conditions at 37°C with controlled humidity and CO_2 levels for 24 hours to facilitate optimal cell attachment and proliferation. Following treatment with various concentrations of fullerene (0, 5, 10, and 15 µg/ml) for 1 hour, the plates were exposed to X-rays for 30 minutes. The supernatant was then collected under a laminar flow hood for analysis. The plate was equilibrated to room temperature. A measured volume of 50 µL of both calibration controls and test specimens was meticulously introduced into each well of the microplate to guarantee accuracy and consistency in the assay setup. The microplate was covered and held on a shaker for 1 hour. Subsequently, the wells were flushed three times with buffered washing solution. An appropriate volume of the detection antibody conjugate was introduced into each well, followed by incubation at optimal conditions for 1 hour to ensure efficient target binding. Subsequent to a further washing cycle, the Avidin-

HRP conjugate was carefully applied to each well and held for 30 minutes at optimal conditions to facilitate precise and efficient molecular interaction. Following five rigorous washing cycles, the substrate solution was carefully dispensed into each well and subsequently held under defined incubation conditions for 15 minutes to enable optimal enzymatic reaction and chromogenic signal development. Ultimately, the reaction-terminating reagent was dispensed into the wells to halt enzymatic activity, and the absorbance was then recorded at 450 nm utilizing a spectrophotometric microplate reader. All experiments were performed three times independently (n = 3 independent biological replicates), with each condition tested in quadruplicate (4 technical replicates) within each independent experiment. Data are presented as mean ± standard deviation (SD) derived from the three independent experiments.

2.8. TNF-α assay (Detection and Quantification of TNF-α Levels Using ELISA)

Cells were seeded into 96-well microplates containing culture medium supplemented with 10% fetal bovine serum (FBS) and incubated at 37°C in a humidified atmosphere with 5% CO_2 for 24 hours to support optimal cell viability and growth. They were subsequently exposed to fullerene (0, 5, 10, 15 µg/mL) for 1 hour and exposed to X-rays for 30 minutes. Afterward, the supernatants were collected under a laminar flow hood and transferred to a new 96-well plate for TNF-α analysis. TNF-α concentrations were quantified through the application of a commercially obtained ELISA kit (Karmania Pars Gene, Iran) in accordance with the manufacturer's guidelines. Briefly, 60 µL of standards with decreasing concentrations and 60 µL of samples were introduced into the microplate wells. The well plate underwent incubation on a rotary shaker at 34°C for two hours. After incubation, the wells were washed three times with diluted wash buffer. Subsequently, 60 µL of the marker antibody were introduced, followed by incubation of the plate at ambient temperature for one hour. Following another washing step, 60 µL of Avidin-HRP were dispensed into the wells and allowed to react for 30 minutes at standard laboratory temperaturewere dispensed into the wells and allowed to react for 30 minutes at standard laboratory temperature. After performing five rinsing cycles, 60 µL of the chromogenic solution was applied to the wells and left to incubate for a period of 15 minutes. In the final step, 30 µL of the stopping reagent was introduced, and optical density was recorded at 455 nm employing a microplate spectrophotometer. All experiments were performed three times independently (n = 3 independent biological replicates), with each condition tested in quadruplicate (4 technical replicates) within each independent experiment. Data are presented as mean ± standard deviation (SD) derived from the three independent experiments.

3. Results

3.1. FE-SEM Characterization of C_{60} fullerene

The nanoscale morphology and surface characteristics of C60 fullerene particles were examined through field emission scanning electron microscopy (FE-SEM). As depicted in Figure 1A, analysis of the FE-SEM images revealed that the particles are spherical with an average size of 56.8 nanometers.

3.2. FTIR analysis

Figure 1B depicts the infrared spectra of the synthesized C60 fullerene nanoparticles. The broad absorption band observed around 3419 cm^{-1} may also arise from hydroxyl groups of adsorbed moisture or residual solvent, and thus might not be intrinsic to the C60 structure, along with peaks at 1527.62 cm^{-1} (C=C), 1421.54 cm^{-1} (C–OH), and 1172.72 cm^{-1} (C–O). These spectral features have been previously identified as characteristic of C60 fullerene.

3.3. XRD analysis

Figure 1C depicts the characteristic diffraction peaks observed at 2θ values of 10.8°, 17.7°, and 20.8°, confirming the formation of pure C60 structures.

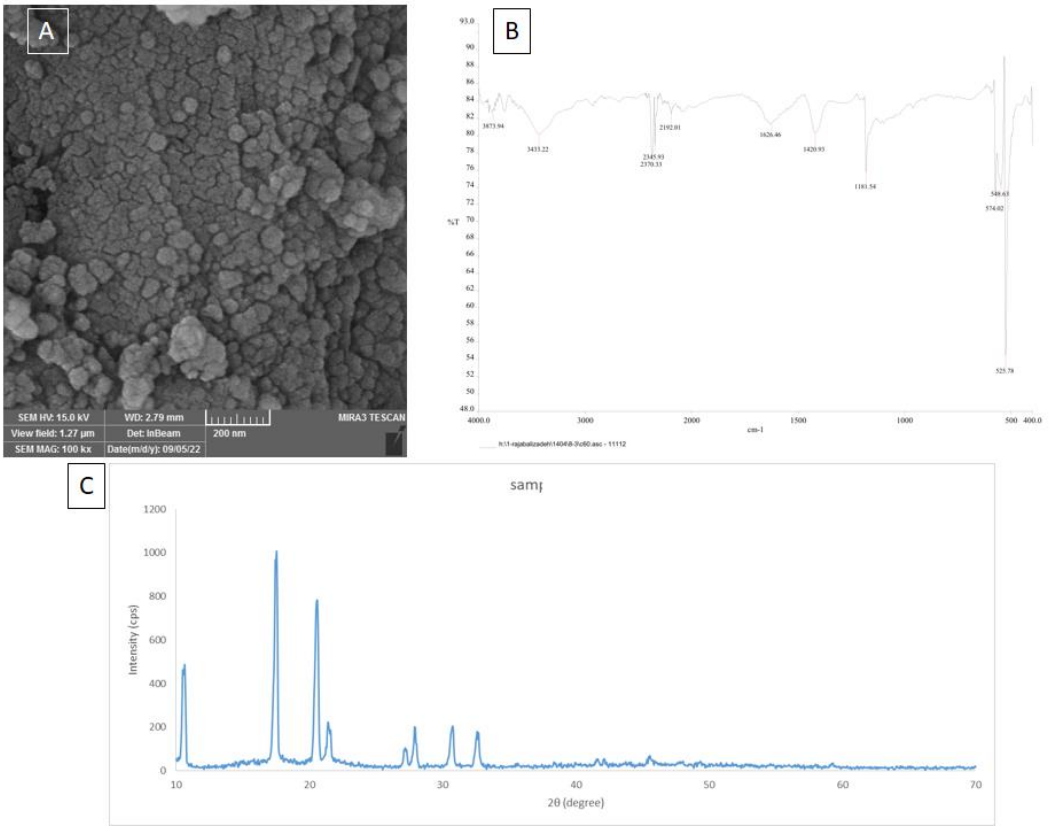

Fig. 1. Structural and Analytical Features of C60 Fullerene Nanoparticles. (A) Field Emission Scanning Electron Microscopy (FE-SEM) image illustrating the morphology of C60 fullerene nanoparticles. (B) Fourier Transform Infrared (FTIR) spectrum indicating functional groups associated with C60 structure. (C) X-ray Diffraction (XRD) pattern reflecting the crystalline structure of the nanoparticles.

3.4. Viability test

The results of the MTT test, which was performed to assess the viability of cells, indicated that exposure to X-rays in the negative control group led to a significant decrease in cell viability compared to the control group without radiation (*$p < 0.05$; Fig. 2). In cells treated with fullerene nanoparticles, a dose-dependent increase in viability was observed. Treatment with 5 and 15 µg/ml of fullerene resulted in a highly significant increase in viability compared to the negative control (***$p < 0.001$; Fig. 2), while the 10 µg/ml dose also showed a significant increase (**$p < 0.01$; Fig. 2). This increase suggests that the presence of fullerene substantially mitigated the cytotoxic effects induced by X-ray radiation (Fig. 2).

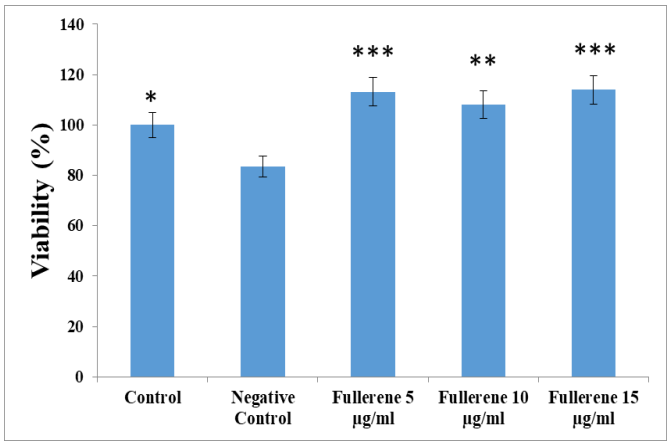

Fig. 2. Percentage of cell viability after treatment with different concentrations of fullerene (5, 10, and 15 µg/mL) compared to the negative control group. Data are reported as mean ± standard deviation (n=3). Asterisks (*, **, ***) indicate statistically significant differences compared to the negative control ($p < 0.05$, $p < 0.01$, and $p < 0.001$, respectively).

3.5. Nitric oxide Test

The results of a test measuring nitric oxide, which is released as a free radical in the immune response, indicate that when fullerene nanoparticles were used as a radioprotector, the amount of nitric oxide decreased compared to the negative control group, that is, when cells were exposed to radiation without fullerene nanoparticles. And as the dose of fullerene nanoparticles used increased, the amount of nitric oxide produced decreased (Fig. 3).

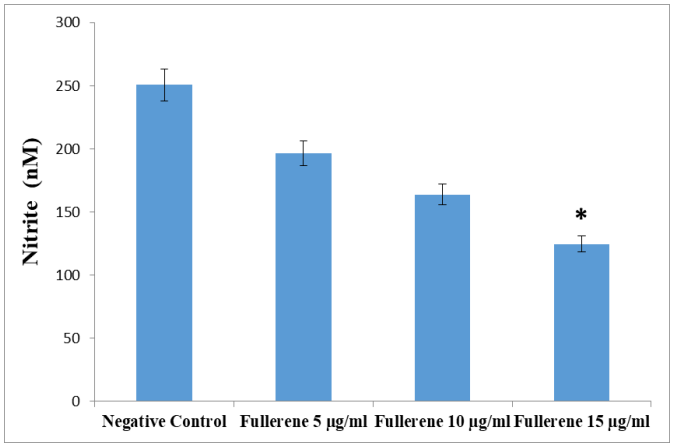

Fig. 3. Nitrite concentration (nM) in cells treated with different concentrations of fullerene (5, 10, and 15 µg/mL) compared to the negative control group. Data are presented as mean ± standard deviation (n=3). The asterisk (*) indicates a statistically significant reduction compared to the negative control ($p < 0.05$).

3.6. IL-6 test

The results of the IL-6 assay, which is a key interleukin involved in inflammatory and immune responses, indicate that treatment with fullerene nanoparticles reduced IL-6 levels in a concentration-dependent manner. Compared to the negative control group (39.5 ± SD pg/ml), fullerene at 5 µg/ml decreased IL-6 to 26.0 pg/ml, at 10 µg/ml to 24.5 pg/ml, and at 15 µg/ml to 17.0 pg/ml. Statistical analysis revealed that the reduction at 15 µg/ml was statistically significant compared to the negative control ($p < 0.05$). Although IL-6 levels were lower in the 5 and 10 µg/ml groups relative to the control, these differences did not reach statistical significance ($p > 0.05$; Fig. 4).

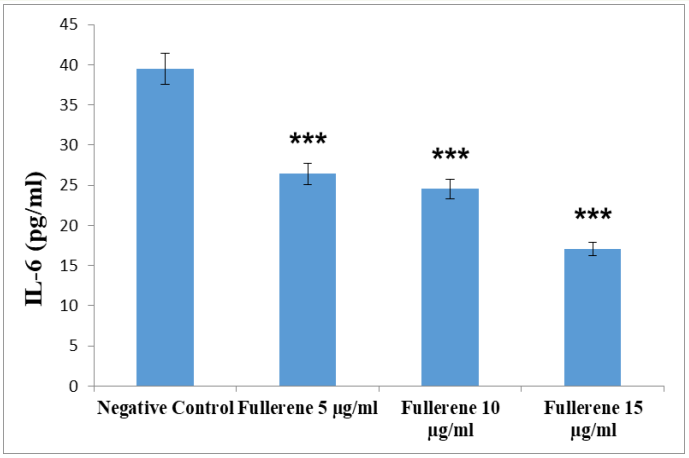

Fig. 4. IL-6 concentration (pg/ml) in cells treated with different concentrations of fullerene (5, 10, and 15 µg/ml) compared to the negative control group. Data are presented as mean ± standard deviation (n=3). The asterisk (***) indicates a statistically significant reduction compared to the negative control ($p < 0.001$).

3.7. TNF-α test

The results of the TNF-α test, which is a useful tool for assessing inflammatory responses, indicate that when fullerene nanoparticles were used as a radioprotectant, the amount of TNF-α was reduced compared to the negative control group in which cells were exposed to radiation without fullerene nanoparticles. And as the dose of fullerene nanoparticles used increased, the amount of TNF-α produced decreased. That is, depending on the increase in the dose of fullerene used, the inflammatory response decreased (Fig. 5).

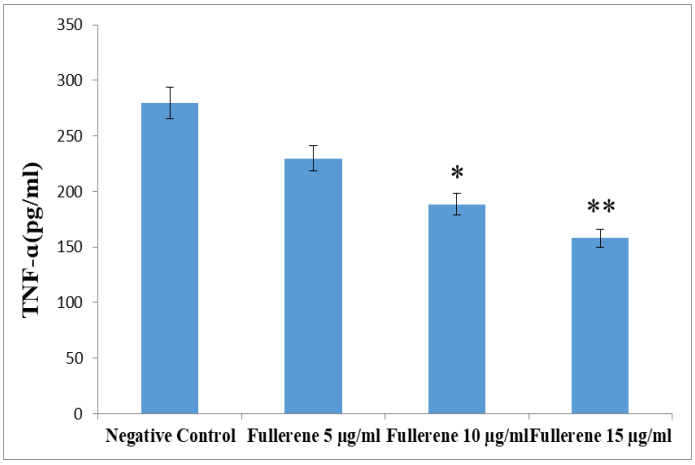

Fig. 5. TNF-α concentration (pg/ml) in cells treated with different concentrations of fullerene (5, 10, and 15 µg/ml) compared to the negative control group. Data are presented as mean ± standard deviation (n=3). Asterisks (*, **) indicate statistically significant differences compared to the negative control ($p < 0.05$ and $p < 0.01$ respectively).

4. Discussion

Adipose tissue is the most widespread connective tissue in humans, originating from the mesodermal germ layer and existing mainly in the form of subcutaneous and visceral fat.[18] One of the complications of radiotherapy for cancer treatment is exposure to adipose tissue, which may increase tissue toxicity.[19] To examine the effect of viability, cells are cultured, exposed to radiation, and re-cultured to examine population doubling time (PDT). Cell survival after irradiation indicates the ability of stem cells to resist external stresses. Exposure to radiation induces both genetic and epigenetic alterations in mesenchymal stem cells, leading to DNA damage, cell cycle arrest, cellular senescence, and ultimately apoptosis. Radiation's impact on mesenchymal stem cells is influenced

by a number of factors such as radiation dose, endogenous cell/tissue, and environmental conditions.[20] Cellular and tissue damage results from direct ionization of macromolecules or some indirect processes via free radicals resulting from the radioactive decomposition of water.[21] Ionization and interaction with free radicals can change the arrangement and roles of DNA, lipids, and proteins.[22]

The study's findings emphasize the intriguing potential of fullerene nanoparticles (C60) as radioprotective agents for reducing the adverse effects of X-ray radiation on adipose-derived stem cells. The discovered protective properties, such as increased cell viability, decreased oxidative stress, and decreased inflammatory responses, lay a solid foundation for further research into C60 nanoparticles in regenerative medicine and radiation protection. Li et al. found that large dosages of radiation considerably impaired the capacity for differentiation, though not totally.[23] According to findings by Pawlik and colleagues, the susceptibility of cells to radiation varies depending on the specific phase of the cell cycle they are in. Cells were especially sensitive throughout the M and G2 phases but comparatively resistant toward the end of the S phase.[24] Furthermore, Korpinski and colleagues suggested that mesenchymal stem cells exhibit a favorable response to radiation by effectively repairing DNA lesions.[25] Finally, the reduced vitality of the groups following radiation and culturing may be associated with the aging of the mesenchymal stem cells themselves.[22] Carbon nanospheres, known as fullerenes, and their soluble in water derivatives exhibit antioxidant capabilities that minimize DNA damage in irradiated cells.[26] Fullerenes are powerful antioxidants that react easily and rapidly with free radicals, which are frequently the root cause of harm to cells or death.[13]

Fullerene nanoparticles are broadly recognized for their potential antioxidant properties through free-radical scavenging, and have been proposed to act as “radical sponges” capable of neutralizing multiple reactive oxygen species.[27] In this study, treatment with C60 nanoparticles led to a significant decrease in nitric oxide (NO) levels. Given that NO can reflect oxidative stress under certain conditions, this observation is consistent with the suggested antioxidant activity of fullerenes and supports previous findings indicating that C60 may modulate reactive nitrogen species (RNS) generation. Nevertheless, because NO also serves as a key signaling molecule, its reduction may involve pathways beyond oxidative stress regulation. Moreover, the absence of direct measurements of ROS or other oxidative stress markers (e.g., glutathione status, lipid peroxidation) limits the ability to confirm an antioxidant mechanism. Therefore, while the “radical sponge” hypothesis remains plausible, future studies incorporating direct oxidative stress assays are required to substantiate this interpretation.[28]

Borbala Darocsi and colleagues investigated the radioprotective potential of DF-1 in Danio rerio embryos. They were subjected to ionizing radiation challenge (10–40 Gy) in the presence and absence of DF-1, followed by evaluation of survival, morphology, and organ functions including renal excretory activity and sensory nerve development. DF-1 at a concentration of 100 µmol/L exhibited no cytotoxicity across the tested range of 1–1,000 µmol/L. Administration of DF-1 within a time window spanning three hours prior to and up to 15 minutes following ionizing radiation exposure markedly mitigated radiation-induced abnormalities, including axial malformations, neurotoxic effects, compromised excretory system function, and reduced organismal viability. The radioprotective potential of DF-1 was comparable to that of amifostine (4 mmol/L), a benchmark radioprotective drug recognized by the FDA, and was primarily attributed to a significant decrease in reactive oxygen species generation. These findings highlight DF-1’s antioxidant properties as a mechanism for mitigating radiation-induced damage. However, it should be noted that the concentration of DF-1 used in that study (100 µmol/L) is considerably higher than the concentration range employed in our work (0–15 µg/mL). Direct

quantitative comparison between the two studies should therefore be made with caution. The observed differences in bioactivity may be influenced by concentration-dependent factors such as solubility, cellular uptake, or the degree of reactive oxygen species scavenging. Nevertheless, the qualitative trend—namely, the antioxidant-mediated mitigation of radiation-induced damage—remains consistent with our findings.[29]

Inflammation is another major consequence of radiation exposure, often mediated by cytokines such as IL-6 and TNF-α. Our findings revealed a dose-dependent drop in the levels of these inflammatory markers following treatment with C60 nanoparticles, indicating anti-inflammatory capabilities. This is consistent with previous research demonstrating the involvement of fullerenes in moderating inflammatory responses by interfering with cytokine signaling pathways. Anthony L. Dellinger and colleagues evaluated the anti-inflammatory effects of fullerene derivatives. They demonstrated that specific derivatives suppressed FcγR- and TNF-α-driven secretory activity in mast cells, synovial fibroblasts, and osteoclasts by decreasing mitochondrial membrane potential, reducing oxygen-derived free radicals, and downregulating NF-κB pathway activation. In vivo investigations employing arthritis models demonstrated that the selected derivatives (ALM and TGA) preferentially accumulated in affected articulations, leading to attenuation of inflammatory responses, prevention of cartilage and bone degradation, and a significant decrease in serum TNF-α concentrations. Importantly, their effects persisted in MC-deficient mice, suggesting broader cellular targets. These findings position fullerene derivatives as promising tools for arthritis therapy and diagnostics.[30]

Notwithstanding these promising results, more research is needed to understand the precise biological pathways underlying C60 nanoparticles' radioprotective actions. Future research should also investigate the appropriate dosage and delivery techniques for fullerene nanoparticles to optimize therapeutic advantages while reducing potential harm.

5. Conclusions

The study shows that fullerene nanoparticles (C60) can effectively protect adipose-derived stem cells (ASCs) from X-ray radiation by mitigating oxidative stress and inflammation. C60 treatment reduced oxidative stress markers and inflammatory cytokines, demonstrating its antioxidant and anti-inflammatory properties. This research suggests C60 could be used in clinical settings to enhance stem cell therapeutic efficacy in radiation-sensitive treatments. The radioprotective effects of C60 nanoparticles are not fully understood, necessitating further in vivo studies—including efficacy assessments in relevant animal models and mechanistic investigations using ROS-specific fluorescent probes—to elucidate the underlying antioxidant pathways and their translational potential.

Limitation

One limitation of this study is the absence of a positive control, such as a well-established radioprotectant (e.g., amifostine or vitamin E), which restricts the ability to directly benchmark the radioprotective efficacy of C60 against recognized reference agents. Future studies incorporating such controls will allow for more robust comparative evaluation.

Authors' Contribution

Conceptualization: Arash Abdolmaleki, Asadollah Asadi.
Data curation: Golnoosh Goodarzi Fard, Arash Abdolmaleki.
Formal analysis: Asadollah Asadi, Farhad Zolfagharpour.

Funding acquisition: Asadollah Asadi, Golnoosh Goodarzi Fard.
Investigation: Golnoosh Goodarzi Fard, Arash Abdolmaleki, Hussein A. Ghanimi.
Methodology: Arash Abdolmaleki, Asadollah Asadi.
Project administration: Arash Abdolmaleki,
Resources: Golnoosh Goodarzi Fard, Hussein A. Ghanimi, Farhad Zolfagharpour.
Software: Farhad Zolfagharpour, Arash Abdolmaleki, Ezzat Nourizadeh.
Supervision:Arash Abdolmaleki.
Validation:Arash Abdolmaleki, Asadollah Asadi, Golnoosh Goodarzi Fard.
Visualization: Golnoosh Goodarzi Fard, Ezzat Nourizadeh, Aida Nahumi, Hussein A. Ghanimi.
Writing–original draft: Golnoosh Goodarzi Fard, Arash Abdolmaleki.
Writing–review & editing: Golnoosh Goodarzi Fard, Arash Abdolmaleki, Asadollah Asadi, Farhad Zolfagharpour, Hussein A. Ghanimi, Ezzat Nourizadeh, Aida Nahumi.

Ethical Approval

The study does not involve experiments with human participants or animals, and therefore ethical approval was not applicable. Also, The Ethics Committee of Mohaghegh Ardabili University (Iran) accepted all procedures.

Competing Interests

The authors declare that they have no conflicts of interest.

Funding

This study was funded by University of Mohaghegh Ardabili,Ardabil, Iran. No: 16389.

Acknowledgements

We wish to thank all the people at Mohaghegh Ardabili University that helped us with this research.

References

1. Alison MR, Poulsom R, Forbes S, Wright NA. An introduction to stem cells. J Pathol 2002;197(4):419-23. doi: 10.1002/path.1187.

2. Nahumi A, Peymani M, Asadi A, Abdolmaleki A, Panahi Y. Biomechanical evaluation of a sheep tracheal scaffold. Cell Tissue Bank 2024:1-8. doi: 10.1007/s10561-024-10078-5.

3. De Francesco F, Ricci G, D'Andrea F, Nicoletti GF, Ferraro GA. Human adipose stem cells: from bench to bedside. Tissue Eng Part B Rev 2015;21(6):572-84. doi: 10.1089/ten.TEB.2014.0609.

4. Pittenger MF, Mackay AM, Beck SC, Jaiswal RK, Douglas R, Mosca JD, et al. Multilineage potential of adult human mesenchymal stem cells. Science 1999;284(5411):143-7. doi: 10.1126/science.284.5411.143.

5. Izadpanah R, Trygg C, Patel B, Kriedt C, Dufour J, Gimble JM, et al. Biologic properties of mesenchymal stem cells derived from bone marrow and adipose tissue. J Cell Biochem 2006;99(5):1285-97. doi: 10.1002/jcb.20904.

6. Abdolmaleki A, Asadi A, Taghizadeh Momen L, Parsi Pilerood S. The role of neural tissue engineering in the repair of nerve lesions. Neurosci J Shefaye Khatam 2020;8(3):80-96. doi: 10.52547/shefa.8.3.80.

7. Nahumi A, Peymani M, Asadi A, Abdolmaleki A, Panahi Y. Decellularized tracheal scaffold as a promising 3D scaffold for tissue engineering applications. Tissue Cell 2023;85:102258. doi: 10.1016/j.tice.2023.102258.

8. Abdolmaleki A, Ghayour MB, Behnam-Rassouli M. Protective effects of acetyl-l-carnitine against serum and glucose deprivation-induced apoptosis in rat adipose-derived mesenchymal stem cells. Cell Tissue Bank 2020;21(4):655-66. doi: 10.1007/s10561-020-09846-2.

9. Qin Y, Ge G, Yang P, Wang L, Qiao Y, Pan G, et al. An update on adipose-derived stem cells for regenerative medicine: where challenge meets opportunity. Adv Sci 2023;10(20):2207334. doi: 10.1002/advs.202207334.

10. Prise KM, Saran A. Concise review: stem cell effects in radiation risk. Stem Cells 2011;29(9):1315-21. doi: 10.1002/stem.684.

11. Farhadi A, Zolfagharpour F, Abdolmaleki A, Asadi A, Zabihi A. Protective effects of selenium nanoparticles against X-ray-induced testicular damage in rats: An integrated experimental and Monte Carlo simulation study. Int J Reprod Biomed 2026;23(11):911. doi: 10.18502/ijrm.v23i11.0000.

12. Kreyling WG, Semmler-Behnke M, Chaudhry Q. A complementary definition of nanomaterial. Nano Today 2010;5(3):165-8. doi: 10.1016/j.nantod.2010.04.004.

13. Waqas M, Khadka DB, Khan AHH, Wang YC. Fullerene-driven photocarrier processes in perovskite solar cells: recent advances. Nanoscale 2025;17:15648-75. doi: 10.1039/D5NR01894C.

14. Speranza G. Carbon nanomaterials: Synthesis, functionalization and sensing applications. Nanomaterials 2021;11(4):967. doi: 10.3390/nano11040967.

15. Cataldo F, Da Ros T. Medicinal chemistry and pharmacological potential of fullerenes and carbon nanotubes. Dordrecht: Springer Science & Business Media; 2008. doi: 10.1007/978-1-4020-6845-8.

16. Semenov KN, Charykov NA, Keskinov VA, Piartman AK, Blokhin AA, Kopyrin AA. Solubility of light fullerenes in organic solvents. J Chem Eng Data 2010;55(1):13-36. doi: 10.1021/je9002398.

17. Prylutska S, Grynyuk I, Matyshevska O, Prylutskyy YI, Ritter U, Scharff P. Anti-oxidant properties of C60 fullerenes in vitro. Fullerenes Nanotubes Carbon Nanostruct 2008;16(5-6):698-705. doi: 10.1080/15363830802317114.

18. Gesta S, Tseng YH, Kahn CR. Developmental origin of fat: tracking obesity to its source. Cell 2007;131(2):242-56. doi: 10.1016/j.cell.2007.10.004.

19. Du YR, Dong P, Chen YX, Gang X, Ren ZX, Li XM, et al. Irradiation response of adipose-derived stem cells under three-dimensional culture condition. Biomed Environ Sci 2015;28(8):549-57. doi: 10.3967/bes2015.078.

20. Manda K, Kavanagh JN, Buttler D, Prise KM, Hildebrandt G. Low dose effects of ionizing radiation on normal tissue stem cells. Mutat Res Rev Mutat Res 2014;761:6-14. doi: 10.1016/j.mrrev.2014.04.001.

21. Islam MS, Stemig ME, Takahashi Y, Hui SK. Radiation response of mesenchymal stem cells derived from bone marrow and human pluripotent stem cells. J Radiat Res 2015;56(2):269-77. doi: 10.1093/jrr/rru098.

22. Rahyussalim AJ, Pawitan JA, Kusnadi AR, Kurniawati T. X-ray radiation effect of C-arm on adipose tissue-mesenchymal stem cell viability and population doubling time. Med J Indones 2016;25(1):10-8. doi: 10.13181/mji.v25i1.1248.

23. Li J, Kwong DL, Chan GCF. The effects of various irradiation doses on the growth and differentiation of marrow-derived human mesenchymal stromal cells. Pediatr Transplant 2007;11(4):379-87. doi: 10.1111/j.1399-3046.2006.00673.x.

24. Pawlik TM, Keyomarsi K. Role of cell cycle in mediating sensitivity to radiotherapy. Int J Radiat Oncol Biol Phys 2004;59(4):928-42. doi: 10.1016/j.ijrobp.2004.03.005.

25. Kurpinski K, Jang DJ, Bhattacharya S, Rydberg B, Chu J, So J, et al. Differential effects of x-rays and high-energy 56Fe ions on human mesenchymal stem cells. Int J Radiat Oncol Biol Phys 2009;73(3):869-77. doi: 10.1016/j.ijrobp.2008.10.002.

26. Vávrová J, Řezáčová M, Pejchal J. Fullerene nanoparticles and their anti-oxidative effects: a comparison to other radioprotective agents. J Appl Biomed 2012;10(1):1-8. doi: 10.2478/v10136-012-0001-5.

27. Malekzadeh D, Asadi A, Abdolmaleki A, Dehghan G. Neuroprotection of fullerene in improving cognitive-behavioral disruptions and neurobiochemical enzymes activities. Nanomedicine 2023;18(6):525-39. doi: 10.2217/nnm-2022-0365.

28. Misirkic MS, Todorovic-Markovic BM, Vucicevic LM, Janjetovic KD, Jokanovic VR, Dramicanin MD, et al. The protection of cells from nitric oxide-mediated apoptotic death by mechanochemically synthesized fullerene (C60) nanoparticles. Biomaterials 2009;30(12):2319-28. doi: 10.1016/j.biomaterials.2008.12.065.

29. Daroczi B, Kari G, McAleer MF, Wolf JC, Rodeck U, Dicker AP. In vivo radioprotection by the fullerene nanoparticle DF-1 as assessed in a zebrafish model. Clin Cancer Res 2006;12(23):7086-91. doi: 10.1158/1078-0432.CCR-06-1421.

30. Dellinger AL, Cunin P, Lee D, Kung AL, Brooks DB, Zhou Z, et al. Inhibition of inflammatory arthritis using fullerene nanomaterials. PLoS One 2015;10(4): e0126290. doi: 10.1371/journal.pone.0126290.